



**HAL**  
open science

## Effect of size, concentration, and nature of fillers on crystallinity, thermal, and mechanical properties of polyetheretherketone composites

Marie Doumeng, Florentin Berthet, Karl Delbé, Olivier Marsan, Jean Denape,  
France Chabert

### ► To cite this version:

Marie Doumeng, Florentin Berthet, Karl Delbé, Olivier Marsan, Jean Denape, et al.. Effect of size, concentration, and nature of fillers on crystallinity, thermal, and mechanical properties of polyetheretherketone composites. *Journal of Applied Polymer Science*, 2022, 139 (5), pp.51574. 10.1002/app.51574 . hal-03333849

**HAL Id: hal-03333849**






<https://imt-mines-albi.hal.science/hal-03333849v1>

Submitted on 15 Sep 2021

**HAL** is a multi-disciplinary open access archive for the deposit and dissemination of scientific research documents, whether they are published or not. The documents may come from teaching and research institutions in France or abroad, or from public or private research centers.

L'archive ouverte pluridisciplinaire **HAL**, est destinée au dépôt et à la diffusion de documents scientifiques de niveau recherche, publiés ou non, émanant des établissements d'enseignement et de recherche français ou étrangers, des laboratoires publics ou privés.

# Effect of size, concentration, and nature of fillers on crystallinity, thermal, and mechanical properties of polyetheretherketone composites

Marie Doumeng<sup>1,2</sup> | Florentin Berthet<sup>2</sup>  | Karl Delbé<sup>1</sup>  | Olivier Marsan<sup>3</sup>  |  
Jean Denape<sup>1</sup>  | France Chabert<sup>1</sup> 

<sup>1</sup>Laboratoire Génie de Production (LGP), INP-ENIT, University of Toulouse, Tarbes, France

<sup>2</sup>Institut Clément Ader (ICA), CNRS, IMT Mines Albi, INSA, ISAE-SUPAERO, UPS, University of Toulouse, Albi, France

<sup>3</sup>CIRIMAT, INP-ENSIACET, University of Toulouse, Toulouse, France

## Correspondence

France Chabert, Laboratoire Génie de Production (LGP), INP-ENIT, University of Toulouse, 47 Avenue d'Azereix, 65016 Tarbes, France.  
Email: france.chabert@enit.fr

## Funding information

Occitanie region; Université de Toulouse

## ABSTRACT

Polyetheretherketone (PEEK) composites exhibit high stiffness, chemical stability, and heat resistance and they are therefore employed in applications under severe operating environments. This work aims to provide insight into the effect of the size, concentration, and type of fillers on the thermal and mechanical properties of PEEK. A total of 32 composites are used to highlight the influence of nature (lamellae, such as boron nitride and graphite and silicon carbide and alumina), size (nano and micrometric), and content (2.5, 5, 7.5, and 10 vol%) of fillers. The melting temperature and lamellar thickness did not change regardless of the nature of the filler. The thermomechanical analysis demonstrates that lamellar fillers form a percolating network and contribute significantly to the enhancement of the storage modulus. The increase in the storage modulus is proportional to the filler content, and it is more pronounced for micro composites. As expected, the percolating network is formed at lower concentrations for lamellar fillers than for spherical ones. The highest conductivity is achieved with graphite at  $0.823 \text{ W m}^{-1} \text{ K}^{-1}$ , which is twice that of PEEK for 10 vol%. Moreover, the use of micrometric fillers results in thermal conductivity enhancement attributed to the higher amount of efficient hot zones for heat transfer.

## KEYWORDS

composites, crystallinity, rheology, thermal conductivity, thermal transition

## 1 | INTRODUCTION

Polymer composites are manufactured by incorporating fillers into a polymer matrix. Composites target many desirable properties including wear resistance, thermal properties, mechanical strength, and formability, which cannot be achieved by the pure matrix alone. The properties of composites are governed by the properties of each constituent and their interfacial interactions. In nanocomposites, the contact surface is higher between the matrix and the filler at a fixed filler loading, which

makes the role of such an interface predominant. This role is even more dominant as the particle size decreases. When switching from a micro filler to a nanometric one, the specific surface increases by a factor of 1000 for spherical shapes, and many studies have focused on predicting how the chemistry and morphology of the matrix synergize with the surface chemistry, size, and shape of nanoscale fillers to define the properties of the resulting material.

The properties of polymer composites depend on the chemical nature, dimensions, and shapes of the fillers.

The other parameters are the volume fractions and distribution of the fillers in the compound. The size and shape of the particles and their surface chemistry influence the interactions at the polymer/filler interface. The volume of the material affected by these interactions constitutes the interphase, that is, a volume where macromolecules are disturbed by the presence of fillers. In this zone, the mobility of the macromolecules, degree of crystallinity, entanglement rate, and degree of crosslinking for thermosetting polymers are different from those of the bulk, which lead to the gradation of properties between the two areas. It is commonly assumed that this phenomenon results from the creation of weak bonds, such as van der Waals and donor-acceptor interactions, which is the case with hydrogen bonds<sup>1</sup>. Numerous studies on polymer fibers presented in the review by Liu and Kumar<sup>2</sup> suggest that the incorporation of carbon nanotubes (CNTs) enhances mechanical properties by the formation of a more ordered, more crystalline, and better-oriented interphase than the rest of the matrix. This interphase is crucial for the performance of the material, as it improves the load transfer from the polymer matrix to the fillers to fully utilize the higher rigidity of the particles. Further, interfacial interactions improve the properties of the polymer because the ordered interphase layer itself will have much better mechanical properties than the rest of the matrix. Polyaryletherketones (PAEK) offer a unique combination of properties and ease of processing, and they are used in highly demanding applications, such as medical, automotive, and aerospace industries. Indeed, PAEK are semi-crystalline thermoplastics that have been launched in the market since the 1980s. Its polymerization occurs via nucleophilic substitution obtained by polycondensation between 200°C and 400°C. Monomers were biphenyl(hydroquinone) and a fluorinated aromatic compound in a polar aprotic solvent (diphenylsulfone). Fluorinated derivatives are preferred for this synthesis because of their better reactivity and higher electronegativity than chlorinated derivatives.<sup>3</sup> The resulting polymer was a copolymer with ether and ketone groups separated by aromatic rings. PEEK, with an ether/ketone ratio of 2, is a widely used high-performance thermoplastic. Not only their heat resistance, chemical resistance, and stiffness are the highest of the thermoplastics range, but they also have demonstrated the best tribological properties, which makes PEEK suitable for moving parts with high friction rates.<sup>4</sup> Owing to these convincing properties, PEEK is used as a matrix in high-performance composites. Despite its strong performance, other properties can be achieved by adding fillers to the PEEK matrix.

In previous studies, long fibers—most often carbon fibers<sup>5</sup> or glass fibers<sup>4</sup>—are associated with the PEEK matrix. In addition, lamellar or particulate reinforcements such as graphite,<sup>6,7</sup> (Sukumaran, Schlarb, and

Baets), molybdenum disulfide,<sup>8</sup> silicon carbide,<sup>9</sup> silicon oxide,<sup>10</sup> and titanium silicocarbide<sup>11,12</sup> have been incorporated. In other cases, it has been proved that polymer blends, through the addition of polyethersulfone<sup>13</sup> and polyetherimide<sup>14</sup> fillers, enhance the thermomechanical properties of PEEK. These results indicate that the thermomechanical properties of PEEK vary depending on the filler size,<sup>15–19</sup> filler rates,<sup>20–24</sup> and filler types.<sup>8,25</sup>

In terms of the thermal properties of any polymer, PEEK exhibits a low thermal conductivity  $\lambda$ . In some cases, such as in milling or drilling, a better heat transfer is suitable for releasing the heat regenerated by wear. The  $\lambda$  for PEEK is  $0.4 \text{ W m}^{-1} \text{ K}^{-1}$ . Adding fillers with a higher  $\lambda$  than the matrix increases the  $\lambda$  of the composites. For instance,  $\lambda$  reaches  $1.2 \text{ W m}^{-1} \text{ K}^{-1}$  with 30 vol% of boron nitride in polyethylene, which is another semi-crystalline polymer.<sup>26</sup> Zhou<sup>27</sup> highlighted a higher  $\lambda$  with boron nitride particles of  $0.5 \mu\text{m}$  compared to  $15 \mu\text{m}$  at the same volume rate. As the surface energy of the smaller particles is higher, the absorption energy between the fillers and matrix increases. Moreover, the thermal conductivities of the amorphous and crystalline phases of a polymer are different. Puertolas<sup>28</sup> established that the evolution of  $\lambda$  follows the evolution of the degree of crystallinity. This stems from the ordering of the polymeric chains; the latter are well ordered and more compact in the crystalline phase, which facilitates heat transfer.

Finally, as expected, the mechanical properties of fillers with a high modulus act as reinforcements, thereby increasing the storage modulus. For instance, at 50°C, Kadiyala<sup>29</sup> noticed an increase of the storage modulus from 3.01 GPa for the pure PEEK to 4.22 GPa with the addition of 10 wt% of silicon carbide. When adding a higher rate, the storage modulus decreases because the fillers are more agglomerated with an insufficient polymer to bind them. Its elongation and fracture resistance decrease with an increase in the filler loading. The presence of a stronger interface formed between the matrix and fillers increases the storage modulus.<sup>30</sup>

Despite these attempts, general conclusions based on these works are unreliable for two reasons: each work focuses on one type of filler, implying that it is difficult to compare the results with each other. The method of elaboration of composites is different in each study; again, this can explain the difference in properties observed when comparing the results.<sup>25,31</sup> Even if undeniable knowledge has been reached through prolific literature on nanocomposites, these results cannot be transposed to PEEK. Indeed, the behavior of such high-performance polymers is specific because of the high rigidity of their macromolecular chains. In this study, we intend to provide more insight into the effect of fillers on the properties of PEEK composites by comparing four fillers and two sizes for each type. We aim

to link the nature, size, and content of the fillers to the crystallinity, thermal conductivity, and thermomechanical properties of the PEEK composites. Therefore, PEEK composites with micrometric and nanometric fillers are prepared by melt mixing. The fillers are lamellar compounds (boron nitride and graphite) and ceramic particles (alumina and silicon carbide). We chose the concentration of fillers between 2.5 and 10 vol%. The lowest concentration at 2.5 vol% is defined by the aim of reaching the percolation threshold to enhance the  $\lambda$  of the composites. The highest concentration at 10 vol% was limited by the increase in viscosity. Indeed, at a high filler loading, the viscosity of the composite increased so much that the dispersion of the particles was not homogeneous. Such blends were excluded from the samples. This percolation question is crucial for controlling the properties of the composites. Even if some models predict the concentration of the percolation threshold, these models assume the same size and shape for all particles. The difficulty is that particle sizes are affected by the preparation process. We measured the initial size distribution using laser granulometry for the eight types of fillers. Then, the filler size distribution after the blending step was calculated by image analysis from the scanning electron microscopy (SEM) images. The results indicated a large size distribution. In addition, the percolation threshold depends on the temperature, as suggested by Abbasi et al.<sup>32</sup> The percolation threshold is different whether we are interested in mechanical, electrical, or thermal percolation. The composites were characterized by differential scanning calorimetry (DSC), X-ray diffractometry (XRD), and density measurements to assess the degree of crystallinity and morphology. The viscoelastic properties of the composites were determined by rheometry, and the thermal properties were measured using the hot disk method.

## 2 | EXPERIMENTAL

### 2.1 | Materials

PEEK granulates grade 450G (Victrex) were used as the matrix. Some common properties are provided in the datasheet.<sup>33</sup> The fillers used have either particulate (silicon carbide grade  $\beta$ , alumina grade  $\alpha$ ) or lamellar shapes (hexagonal boron nitride and graphite). The references and sizes of the fillers are listed in Table 1. Two sizes were selected for each type of filler: microfillers and nanofillers. The composite samples were labeled as follows: PEEK–type–size–rate. For size, N indicates nanofillers, and M indicates microfillers. As an example, PEEK–BN–N–7.5% refers to a PEEK filled with 7.5 vol% of nanosized boron nitride.

### 2.2 | Preparation of polymer composites

Samples were prepared by blending the matrix in the molten state and the fillers in an internal mixer (Rheomix 600, ThermoFischer) equipped with roller rotors. The mixing was performed at 360°C for 10 min at a rotating speed of 40 rev min<sup>-1</sup>, which corresponds to a mean shearing rate of 40 s<sup>-1</sup>. Based on relevant information from the literature,<sup>34–36</sup> we assume that inorganic fillers are stable under the processing conditions (360°C for 10 min), which means their chemical structures are not changed. According to a previous study,<sup>37</sup> there is no change on the surface of graphite under oxidation at 500°C. The composite material was then removed from the mixer and ground to reach pellets with a maximum dimension of 2 mm. The pellets were then molded into 2-mm-thick plates with a hot press (LAB 800P, Pinette Emidecau Industries). The processing cycle follows three steps: (1) heating until 360°C at 4 K min<sup>-1</sup>, (2) temperature stabilization for 5 min, and (3) cooling to 100°C at 4 K min<sup>-1</sup>. A cooling ramp was selected to achieve the maximum degree of crystallinity of the polymer. The concentrations of fillers  $x_r$  were 2.5, 5, 7.5, and 10 vol%, two sizes, and four types of fillers were studied. A total of 32 composites were prepared to assess the type, size, and rate of the fillers.

### 2.3 | Characterization

SEM observations were performed (EVO HD 15 LS, ZEISS) to measure the filler distribution on the surface of the matrix. The samples were cut into parts of 40 mm × 30 mm × 2 mm. The degree of crystallinity and morphology were determined using three different techniques: density measurements, DSC, and XRD. The density  $\rho$  of the specimens was measured by hydrostatic weight or immersion according to ISO 1183-1:2019. Each sample was weighed at least thrice. The DSC instrument used was Q200 (TA Instruments). Samples were cut to obtain approximately 10 mg of material, placed in sealed aluminum pans, and heated from 80°C to 380°C at 10 K min<sup>-1</sup>. A nitrogen flow at 50 K min<sup>-1</sup> was used to prevent degradation. The temperature was maintained for 1 min at 380°C, and then, the sample was cooled from 380°C to 80°C at 10 K min<sup>-1</sup>, and a second heating ramp was applied. For each sample, at least two analyses were performed to determine the reproducibility of the measurements. The XRD instrument was X'Pert Panalytical (Philips). The measurements were made for  $2\theta$  between 5° and 40° with a step of 0.017°. The diffractometer was equipped with a copper tube ( $\lambda = 0.154$  nm) with an intensity of 40 mA and a voltage of 45 kV. The Hot Disk TPS 2500S analyzer is a device for measuring the thermal

**TABLE 1** References of fillers used in the study. The letter N indicates a nanosize, M indicates a microsize. Size of filler according to the supplier is presented in the table

| Type            | Size ( $\mu\text{m}$ ) |             | Supplier     | Reference |
|-----------------|------------------------|-------------|--------------|-----------|
| Silicon carbide | N                      | 0.050       | GoodFellow   | SI516022  |
|                 | M                      | 0.2–5       | abcr         | B-hp      |
| Alumina         | N                      | 0.005–0.150 | PlasmaChem   | PL-A-AIO  |
|                 | M                      | 1–3         | SumitoChem   | ALM-41    |
| Boron nitride   | N                      | 0.1–1       | PlasmaChem   | PL-H-HBN  |
|                 | M                      | 1–10        | Saint-Gobain | PCTP2     |
| Graphite        | N                      | 0.003       | Avanzare     | av-PLAT-7 |
|                 | M                      | 1–50        | Merck        | 104,206   |

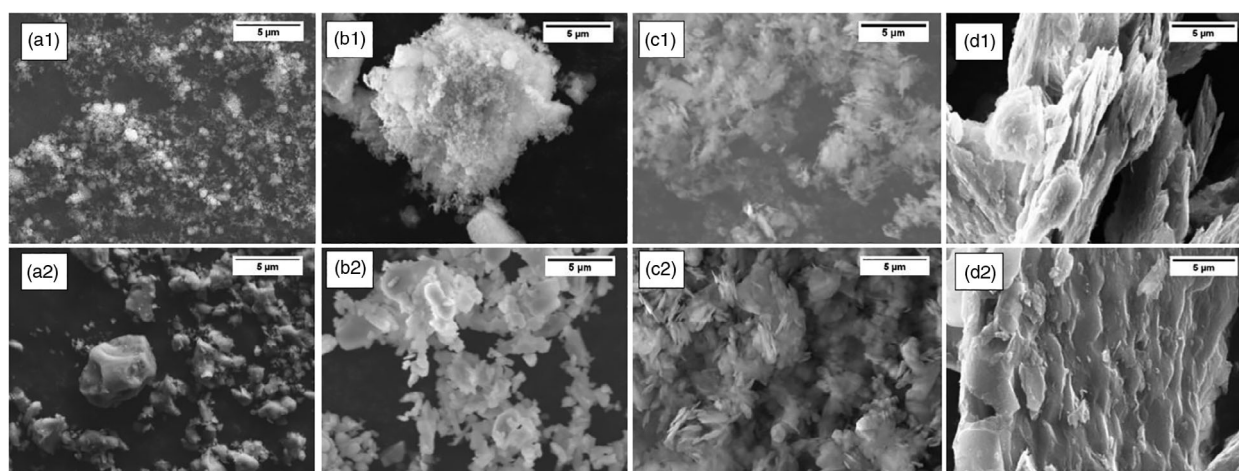


**FIGURE 1** The scanning electron microscopy images of nanofillers (a1,b1,c1,d1) and microfillers (a2,b2,c2,d2) of silicon carbide (a1,a2), alumina (b1,b2), boron nitride (c1,c2) and graphite (d1,d2)

conductivity, thermal diffusivity, and thermal capacity of homogeneous and heterogeneous materials. The probe with a diameter of 2 mm comprises a double nickel spiral electrically insulated by an insulating Kapton coating. The heating power was fixed at 20 mW for 5 s to raise the temperature of the studied material by a few degrees. Each sample, a 3.5-mm-thick plate, is analyzed five times for reproducibility. Dynamic mechanical analysis measures the viscoelastic properties and provides information on the molecular mobility of the polymer chains. A rheometer (ARES LN2, Rheometrics) was used in a rectangular torsion configuration. A fixed deformation of 0.5% at a frequency of 1 Hz was imposed by a motor at the lower part. The sensor connected to the upper part measured the resulting stress in the sample. The sample was heated in a furnace at a temperature ramp of 3 K min<sup>-1</sup>. Each material was tested once to determine the linear viscoelastic domain,

that is, in the range where the stress is proportional to the strain applied by strain sweep at room temperature. Then, a heating ramp was applied within the linear viscoelastic domain from room temperature up to 300°C.

### 3 | RESULTS AND DISCUSSION

#### 3.1 | Characterization of fillers

The fillers formed aggregates before the mixing step (Figure 1). The high shear viscosity of PEEK in the melted state—approximately 5000 Pa s at the Newtonian plateau—generates high stresses on the aggregates, which leads to filler failure and erosion.<sup>38–40</sup> It is known that the dispersion increases with the duration of shear until the creation of a percolating network, which results in a drastic increase in the viscosity at low shear.<sup>41</sup> The

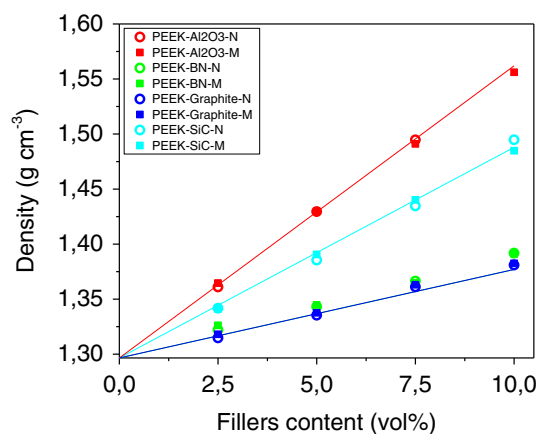
same trend was observed during the preparation of the composites. Composites containing 10 vol% of alumina does not appear homogeneous with the naked eye because of the high viscosity, and therefore, we exclude this formulation from our study. The dispersion state of the composites was quantified through SEM observations in the chemical contrast mode. Images were analyzed using ImageJ to quantify their maximum dimensions in a previous study.<sup>42</sup> The distribution was considered homogeneous for the two studied sizes. Moreover, particulate reinforcements, such as silicon carbide and alumina, have spherical shape and lead to a better dispersion than that with lamellar reinforcements such as boron nitride and graphite.

Figure 2 reveals the density measurements of PEEK ( $\rho = 1.297 \pm 0.005 \text{ g cm}^{-3}$ ) and PEEK composite. The lines correspond to the mixing law, and it precisely follows the experimental results obtained with 2.5–5 to 7.5–10 vol%. This attests that the number of fillers introduced into the polymer corresponds to the expected content.

### 3.2 | Thermal transitions

The characteristic temperatures of PEEK and reinforced PEEK are determined by DSC analyses and presented in Tables 2 and 3.

For PEEK, the glass transition temperature  $T_g$  was  $152.5^\circ\text{C} \pm 0.1^\circ\text{C}$ . The addition of nanometric lamellar fillers such as boron nitride and graphite increases  $T_g$  up to  $160.5^\circ\text{C}$ . For all other sizes and natures of fillers,  $T_g$



**FIGURE 2** Density for samples reinforced with alumina, boron nitride, graphite and silicon carbide. Lines correspond to theoretic density of samples. Absolute uncertainty for density measurement is  $0.005 \text{ g cm}^{-3}$ , not shown on the graph [Color figure can be viewed at [wileyonlinelibrary.com](http://wileyonlinelibrary.com)]

decreases until  $143.1^\circ\text{C}$ . Table 4 compares the characteristic temperatures in the literature;  $T_g$  is unchanged with the addition of reinforcement.  $T_g$  reflects the mobility of the amorphous polymeric phase, which was divided into free and rigid amorphous phases. Near the particle, two scenarios are possible: in the case of good adhesion, the macromolecules are more constrained, which leads to a higher  $T_g$ . In the case of weak adhesion (no chemical interaction), the mobility of the macromolecules is higher, and it decreases  $T_g$ . For lamellar fillers such as boron nitride and graphite, some macromolecules can be trapped between nanolayers; this phenomenon is called exfoliation and these molecules are very rigid. Thus,  $T_g$  is increased. Finally, the contribution of long-distance interactions between particles is responsible for increasing the  $T_g$  of the bulk. All these phenomena competed to yield an average of  $T_g$ . The glass transition indicated in the table is the result of these different contributions.

Figure 3 represents the melting peak of PEEK; the maximum peak is at  $345.1^\circ\text{C} \pm 0.1^\circ\text{C}$ . Further, the melting peak of PEEK is compared to composites reinforced with nanosizes of boron nitride (a) and alumina (b). Other results are provided in Supporting Information. The maximum of the peak is shifted towards higher temperatures compared to pure PEEK. The trend is similar to all other samples whatever the fillers size, concentration, and nature of the fillers, except for the silicon carbide nanofillers. The size and type of fillers have little influence on the melting temperature  $T_m$ , because the melting peak is similarly shifted for almost all formulations. A shift of  $T_m$  to higher temperatures signifies that more energy is required to melt the crystallites. This energy gain can be attributed to the macromolecules being involved in bigger crystalline structures or an interaction between matrix and fillers.

The width of the melting peak decreased with the addition of the filler; this means that the size distribution is reduced and the sizes of the crystallites are close to each other. Bragaglia<sup>47</sup> assigns a width reduction to the fact that there are fewer small crystallites. For all our samples, the peak height decreases with the addition of reinforcement in accordance with the polymer weight decrease when increasing the filler loading while maintaining the same sample weight; therefore, the variation in the heat flow decreases. Although the filler loading is considered to calculate the degree of crystallinity, it does not influence the peak location. Table 4 represents the evolution of the  $T_m$  shift measured by other authors. Some of them highlight a similar increase in  $T_m$ , which is in agreement with our results. Other studies have shown no change in  $T_m$ .<sup>45,48</sup> In our experiments, the maximum shift of  $T_m$  is  $2.6 \pm 0.1 \text{ K}$ , which is low.

**TABLE 2** Comparison of characteristic temperature for samples particular reinforced polyetheretherketone (PEEK).  $T_g$ ,  $T_m$ ,  $T_c$  are respectively the glass transition temperature, the melting temperature and the crystallization temperature. The absolute uncertainty is  $\pm 0.1$  for all the temperatures

| Samples                                | Rate (vol%) | $T_g$ ( $^{\circ}\text{C}$ ) | $T_m$ ( $^{\circ}\text{C}$ ) | $T_c$ ( $^{\circ}\text{C}$ ) |
|--|-------------|------------------------------|------------------------------|------------------------------|
| PEEK                                   | 0           | 152.5                        | 345.1                        | 300.3                        |
| PEEK-SiC-N                             | 2.5         | 148.8                        | 345.0                        | 298.8                        |
|  | 5.0         | 152.2                        | 344.9                        | 295.5                        |
|  | 7.5         | 151.9                        | 344.7                        | 298.1                        |
|  | 10.0        | 149.9                        | 343.3                        | 298.7                        |
|  | 2.5         | 153.4                        | 346.2                        | 300.7                        |
| PEEK-SiC-M                             | 5.0         | 149.3                        | 346.5                        | 299.2                        |
|  | 7.5         | 149.0                        | 347.5                        | 298.1                        |
|  | 10.0        | 148.3                        | 346.8                        | 297.5                        |
|  | 2.5         | 146.0                        | 345.9                        | 293.9                        |
| PEEK-Al <sub>2</sub> O <sub>3</sub> -N | 5.0         | 147.6                        | 344.9                        | 292.8                        |
|  | 7.5         | 147.5                        | 344.7                        | 292.8                        |
|  | 2.5         | 147.4                        | 346.9                        | 299.8                        |
| PEEK-Al <sub>2</sub> O <sub>3</sub> -M | 5.0         | 146.1                        | 347.0                        | 300.2                        |
|  | 7.5         | 147.7                        | 347.7                        | 300.1                        |
|  | 10.0        | 151.5                        | 346.6                        | 300.1                        |

**TABLE 3** Comparison of characteristic temperature for samples lamellar reinforced polyetheretherketone (PEEK).  $T_g$ ,  $T_m$ ,  $T_c$  are respectively the glass transition temperature, the melting temperature and the crystallization temperature. The absolute uncertainty is  $\pm 0.1$  for all the temperatures

| Samples         | Rate (vol%) | $T_g$ ( $^{\circ}\text{C}$ ) | $T_m$ ( $^{\circ}\text{C}$ ) | $T_c$ ( $^{\circ}\text{C}$ ) |
|-----------------|-------------|------------------------------|------------------------------|------------------------------|
| PEEK            | 0           | 152.5                        | 345.1                        | 300.3                        |
| PEEK-BN-N       | 2.5         | 159.8                        | 346.2                        | 300.9                        |
|                 | 5.0         | 150.4                        | 347.2                        | 302.0                        |
|                 | 7.5         | 154.6                        | 345.0                        | 302.9                        |
|                 | 10.0        | 149.3                        | 347.0                        | 302.8                        |
| PEEK-BN-M       | 2.5         | 154.8                        | 346.4                        | 300.5                        |
|                 | 5.0         | 148.4                        | 346.2                        | 299.0                        |
|                 | 7.5         | 143.1                        | 346.6                        | 301.6                        |
|                 | 10.0        | 150.1                        | 346.0                        | 301.9                        |
| PEEK-graphite-N | 2.5         | 160.5                        | 346.9                        | 299.5                        |
|                 | 5.0         | 147.1                        | 346.2                        | 299.6                        |
|                 | 7.5         | 154.2                        | 346.3                        | 300.2                        |
|                 | 10.0        | 148.3                        | 345.6                        | 301.1                        |
| PEEK-graphite-M | 2.5         | 151.1                        | 346.8                        | 301.0                        |
|                 | 5.0         | 153.4                        | 345.8                        | 301.2                        |
|                 | 7.5         | 148.3                        | 347.7                        | 300.9                        |
|                 | 10.0        | 149.2                        | 346.1                        | 301.0                        |

Figure 4 shows the crystallization peak obtained on cooling for PEEK. Its maximum peak occurs at  $300.3^{\circ}\text{C} \pm 0.1^{\circ}\text{C}$ ; the crystallization peak obtained for composites is

shown on the same graph. The nature of the fillers influences the crystallization. The crystallization temperature  $T_c$  is shifted upwards for nanosize boron nitride (a) while  $T_c$  is



**TABLE 4** Comparison of characteristic temperature, degree of crystallinity from various polymer composites for different type, size and rate of reinforcements.  $T_g$ ,  $T_m$ ,  $T_c$ ,  $\chi_c$  are respectively the glass transition temperature, the melting temperature, the crystallization temperature and the degree of crystallinity

| Type                                  | Size ( $\mu\text{m}$ ) | Rate (vol%) | $T_g$ | $T_m$ | $T_c$ | $\chi_c$ |
|---------------------------------------|------------------------|-------------|-------|-------|-------|----------|
| $\text{Al}_2\text{O}_3$ <sup>20</sup> | 0.030                  | 0.8–3.3     |       | →     | ↘     | ↗        |
| $\text{Al}_2\text{O}_3$ <sup>17</sup> | 0.039                  | 0.4–1.6     |       | → ↗   | → ↗   | ↗ →      |
| $\text{Al}_2\text{O}_3$ <sup>16</sup> | 8                      | 1.7–24.4    |       | ↗     | ↗     | ↗        |
| $\text{AlN}$ <sup>43</sup>            | 5                      | 4.2–28.5    |       | ↗     | ↗     | ↗        |
| $\text{BN}$ <sup>44</sup>             | 0.5                    | 1.2–5.1*    | →     | →     | ↗     | →        |
| Graphene <sup>45</sup>                | 0.005                  | 0.6–3.2*    |       | →     | ↘     | ↗ →      |
| Graphene <sup>28</sup>                | 0.010                  | 0.6–6.4*    | →     | →     | ↗     |          |
| Graphene <sup>22</sup>                | 0.003                  | 1.2–3.2*    |       | →     |       | ↗        |
| Graphite <sup>23</sup>                | 10–150                 | 1.2–21.0*   | →     | →     | →     | ↘        |
| $\text{Si}_3\text{N}_4$ <sup>46</sup> | 0.050                  | 1–13.9      |       | ↗ ↘   | ↗ ↘   | ↗ ↘      |
| $\text{SiC}$ <sup>29</sup>            | 0.060                  | 1.2         |       | →     | ↘     | ↗        |
| $\text{SiC}$ <sup>29</sup>            | 20                     | 2.1–9.3     |       |       | ↘     | ↗        |
| $\text{SiO}_2$ <sup>20</sup>          | 0.030                  | 1.2–4.9     |       | →     |       |          |
| $\text{TiO}_2$ <sup>47</sup>          | 0.7                    | 1–5         |       | →     | ↗ ↘   | ↗        |

Note: \* Values converted by considering the density  $\rho$  of boron nitride, graphene and graphite equal to  $2.1 \text{ g cm}^{-3}$ .

**FIGURE 3** DSC thermograms during heating for samples nanoreinforced with (a) boron nitride and (b) alumina [Color figure can be viewed at wileyonlinelibrary.com]

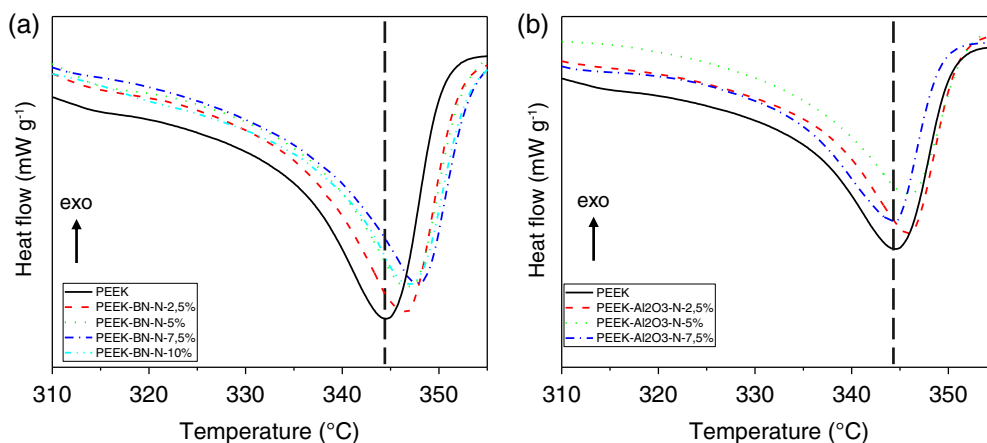
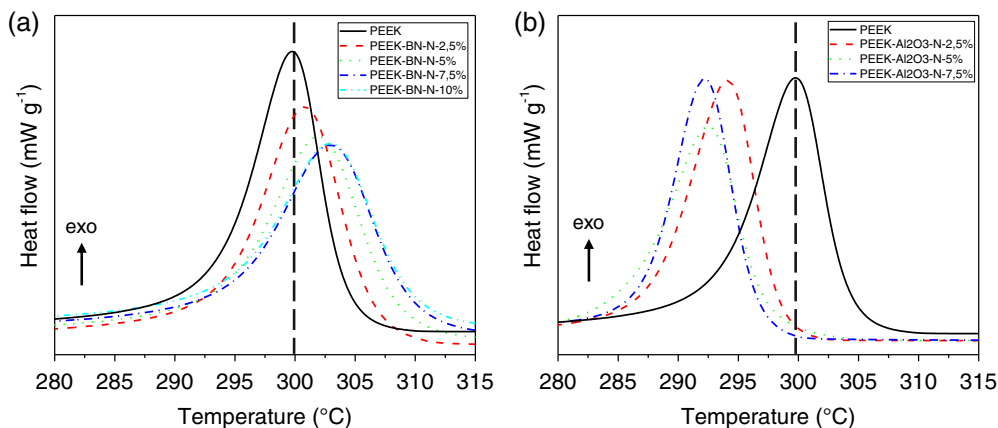


**FIGURE 4** Differential scanning calorimetry thermograms during cooling for samples nanoreinforced with (a) boron nitride and (b) alumina [Color figure can be viewed at wileyonlinelibrary.com]



shifted downwards for nanosize alumina (b). Thus, less energy is required for PEEK macromolecules to self organize into spherulites in the neighborhood of boron nitride nanosheets compared to that for alumina particles. For all

other nature and size of fillers (see Supporting Information), no trend appears concerning  $T_c$ . The values of  $T_c$  of PEEK composites from the literature are listed in Table 4. These data reveal both an increase and decrease of  $T_c$  but



no evident trend for the evolution of  $T_c$ . A few explanations are provided by the authors. For example, Panda<sup>49</sup> explained that a decrease of  $T_c$  is attributed to the presence of fillers that hinder the growth of crystallites. However, this hypothesis does not agree with our previous results about  $T_m$ . He<sup>45</sup> explains  $T_c$  decrease is caused by the formation of more imperfect crystallites. An increase of  $T_c$  can be related to a higher degree of crystallinity. Thus, no significant trend can be observed through the analysis of the DSC thermograms in terms of the nature, size, and rate of the filler. We assume from small variations of  $T_m$  and  $T_c$  that the alumina particles hinder the spherulites growth, whereas boron nitride sheets favor it. These results are observed on nanosize fillers for which the polymer–filler interface is larger.

Let us consider the nature of the filler. Figure 5 represents the melting and crystallization peaks at the same rate of filler, 7.5 vol%; the behavior is more marked for nanosized fillers. In Figure 5a, it is clear that the location of the melting peak is shifted upwards for boron nitride, whereas a little change is observed for the others. The amplitude of the melting peaks is smaller for composites compared to PEEK. When comparing the composites themselves, the amplitude of the melting peak of the nano-alumina composite is very small, whereas the others look similar. Therefore, the degree of crystallinity of the alumina nanocomposites is reduced compared to that of the other samples. Further, the same tendency occurs on cooling with a different behavior observed for alumina: the crystallization peak is shifted downwards and the peak area is smaller. This trend is not clear for  $T_c$  and  $T_m$  because of the nature of the microsized fillers. In Figure 5b, the melting peaks are slightly shifted to higher temperatures, whereas the shift of the crystallization peaks is insignificant considering the uncertainty. For microsized

fillers, the peaks of the alumina composites are considerably larger than those of the others and pure PEEK. In conclusion, thermal transitions did not evolve significantly with the nature of the fillers.

### 3.3 | Lamellar thickness

Changes in crystalline morphology were determined by analyzing the XRD diffractograms. PEEK crystallizes into an orthorhombic cell, for which the dimensions have been reported in the literature.<sup>50</sup> Only alumina-reinforced PEEK is presented in this paper. Figure 6a shows the main diffraction peak positions and alumina composites. The diffraction peaks for pure PEEK are located at 18.79°, 20.72°, 22.66°, and 28.73°, corresponding to the (110), (111), (200), and (210) planes, respectively. The main diffraction peak positions for the Al<sub>2</sub>O<sub>3</sub> powder are (012), (104), and (110) at 25.52°, 35.12°, and 37.73°, respectively. Figure 6a shows the diffractogram of PEEK reinforced with 2.5 vol% nano- and micro-alumina fillers. All main peaks of PEEK and alumina are visible in the diffractograms of the nano- and microcomposites. This indicates no evidence of a different crystalline phase among the composites. In both cases, diffraction peaks were less intense because of the decrease in the polymer amount in these samples. The main difference between the diffractograms of PEEK and those of the composites is the peak position of the (200) plane of PEEK. With the addition of fillers—regardless of the size, type, and rate of reinforcement—the peak position shifted to a higher angular position (Figure 6b), which indicates that a change in the polymer morphology occurs or could be the apparition of constraint in the material. This shift was more pronounced for the nanofilled PEEK. This

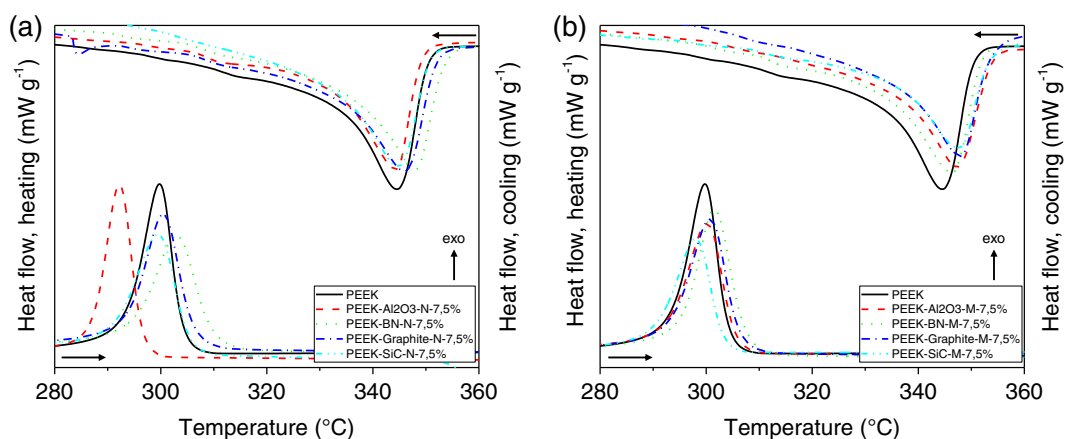
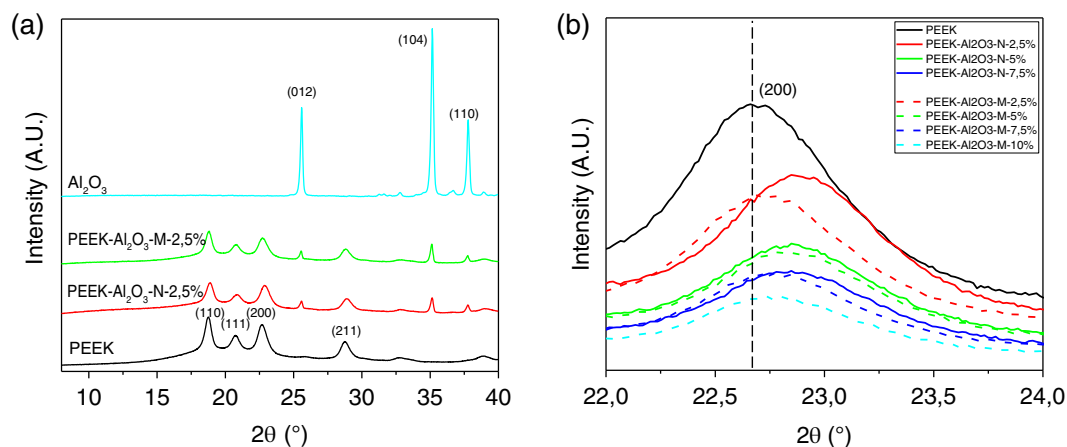


FIGURE 5 Differential scanning calorimetry thermograms for samples reinforced with 7.5 vol% of (a) nanoreinforcement, and (b) microreinforcement of alumina, boron nitride, graphite and silicon carbide [Color figure can be viewed at wileyonlinelibrary.com]



**FIGURE 6** (a) X-ray diffractometry (XRD) diffractogram of pure Polyetheretherketone (PEEK), powder of alumina and PEEK reinforced with 2.5 vol% of nano and microreinforcement of alumina. For clarity the curves are displaced upwards. (b) XRD diffractogram of pure PEEK and PEEK reinforced with reinforcement of alumina [Color figure can be viewed at [wileyonlinelibrary.com](http://wileyonlinelibrary.com)]

**TABLE 5** Properties for particular reinforced polyetheretherketone (PEEK): lamellae thickness  $L_c$  and coherence length  $L_{hkl}$  of the main diffraction peak; degrees of crystallinity  $\chi_c$  by density  $\rho$  measurements, differential scanning Calorimetry (DSC), X-ray diffractometry (XRD); (\*) thermal properties with thermal conductivity  $\lambda$  in  $\text{W m}^{-1} \text{K}^{-1}$ , thermal diffusivity  $D$  in  $\times 10^{-6} \text{m}^2 \text{s}^{-1}$  and heat capacity  $C$  in  $\text{kJ kg}^{-1} \text{K}^{-1}$

| Rate (vol%)                            | Lamellar dimensions |                |                |                |                | $\chi_c$   |         |           | Thermal properties |                        |            |
|--|---------------------|----------------|----------------|----------------|----------------|------------|---------|-----------|--------------------|------------------------|------------|
|  | $L_c$ (nm)          | $L_{110}$ (nm) | $L_{111}$ (nm) | $L_{200}$ (nm) | $L_{210}$ (nm) | $\rho$ (%) | DSC (%) | XRD (%)   | $\lambda$ (*)      | D (*)                  | C(*)       |
|  | $\pm 0.01$          | $\pm 2$        | $\pm 2$        | $\pm 2$        | $\pm 2$        | $\pm 3$    | $\pm 1$ | $\pm 0.5$ | $\pm 0.005$        | $\pm 1 \times 10^{-8}$ | $\pm 0.05$ |
| PEEK                                   |                     |                |                |                |                |            |         |           |                    |                        |            |
| 0                                      | 4.21                | 14             | 14             | 11             | 11             | 25         | 34      | 37.1      | 0.290              | 0.23                   | 9.81       |
| PEEK-SiC-N                             |                     |                |                |                |                |            |         |           |                    |                        |            |
| 2.5                                    | 4.22                | 20             | 15             | 15             | 14             | 23         | 36      | 41.3      | 0.295              | 0.35                   | 6.37       |
| 5.0                                    | 4.23                | 19             | 14             | 15             | 15             | 19         | 31      | 42.1      | 0.324              | 0.36                   | 6.43       |
| 7.5                                    | 4.22                | 19             | 16             | 15             | 16             | 20         | 31      | 41.8      | 0.348              | 0.24                   | 10.00      |
| 10.0                                   | 4.26                | 18             | 17             | 13             | 13             | 30         | 26      | 46.0      | 0.368              | 0.46                   | 5.31       |
| PEEK-SiC-M                             |                     |                |                |                |                |            |         |           |                    |                        |            |
| 2.5                                    | 4.31                | 19             | 14             | 15             | 13             | 22         | 35      | 39.6      | 0.296              | 0.33                   | 6.70       |
| 5.0                                    | 4.38                | 21             | 14             | 14             | 17             | 23         | 30      | 41.0      | 0.340              | 0.26                   | 9.38       |
| 7.5                                    | 4.50                | 18             | 17             | 13             | 15             | 25         | 23      | 40.3      | 0.355              | 0.23                   | 10.49      |
| 10.0                                   | 4.47                | 17             | 16             | 13             | 11             | 22         | 24      | 37.6      | 0.428              | 0.32                   | 8.91       |
| PEEK-Al <sub>2</sub> O <sub>3</sub> -N |                     |                |                |                |                |            |         |           |                    |                        |            |
| 2.5                                    | 4.33                | 17             | 16             | 13             | 14             | 25         | 35      | 43.1      | 0.328              | 0.24                   | 10.24      |
| 5.0                                    | 4.32                | 17             | 16             | 13             | 14             | 25         | 29      | 33.1      | 0.393              | 0.29                   | 9.43       |
| 7.5                                    | 4.25                | 17             | 12             | 14             | 12             | 24         | 28      | 34.6      |                    |                        |            |
| PEEK-Al <sub>2</sub> O <sub>3</sub> -M |                     |                |                |                |                |            |         |           |                    |                        |            |
| 2.5                                    | 4.46                | 19             | 16             | 13             | 15             | 26         | 34      | 33.9      | 0.324              | 0.24                   | 10.05      |
| 5.0                                    | 4.38                | 18             | 15             | 13             | 14             | 25         | 31      | 31.6      | 0.359              | 0.26                   | 9.80       |
| 7.5                                    | 4.46                | 19             | 17             | 13             | 15             | 21         | 30      | 35.2      | 0.394              | 0.27                   | 9.74       |
| 10.0                                   | 4.40                | 19             | 15             | 13             | 12             | 20         | 27      | 34.5      | 0.445              | 0.31                   | 9.38       |

result is corroborated by the evolution of  $T_c$ , for which we highlight more polymer–filler interactions with nanofillers. A hypothesis is that the change in crystalline morphology occurs at the interphase in the neighborhood of the fillers. Even if we did not explore the crystalline morphology at the interface, some authors have proved that the interface acts as a nucleating agent in some cases. For instance, glass fibers allow crystalline growth with a lamellar structure perpendicular to the fibers. This appears when the macromolecular chains have a good affinity for the surface. Zhang showed polymer transcrystallinity in the presence of CNTs in polypropylene using polarized optical microscopy. The transcrystals grew perpendicular to the nanotube fiber axis.

The coherence length  $L_{hkl}$  is evaluated using the Scherrer equation (Equation 1), where  $k$ ,  $\lambda$ ,  $\beta$ , and  $2\theta$

denote Scherrer constant equal to 0.9, wavelength of the X-ray, width at half the intensity of the diffraction peak in radians, and scattering Bragg's angle of the crystalline peak, respectively.

$$L_{hkl} = \frac{k\lambda}{\beta \cos(2\theta/2)}. \quad (1)$$

Tables 5 and 6 show the values of  $L_{hkl}$  for the main diffraction peaks for the PEEK sample and the particulate-reinforced PEEK, respectively. For lamellar-reinforced PEEK, the main diffraction peaks of the fillers correspond to the same angular position of PEEK, and therefore, the exact angular position is difficult to evaluate. The values of  $L_{hkl}$  for these samples were not determined in this study. For PEEK,  $L_{110}$  and  $L_{111}$  are higher than  $L_{200}$  and  $L_{210}$ , and these values are consistent with the literature.<sup>51–54</sup>

**TABLE 6** Properties for lamellar reinforced polyetheretherketone (PEEK): lamellae thickness  $L_c$ ; degrees of crystallinity  $\chi_c$  by density  $\rho$  measurements, differential scanning calorimetry (DSC), X-ray diffractometry (XRD); (\*) thermal properties with thermal conductivity  $\lambda$  in  $\text{W m}^{-1} \text{K}^{-1}$ , thermal diffusivity  $D$  in  $\times 10^{-6} \text{m}^2 \text{s}^{-1}$  and heat capacity  $C$  in  $\text{kJ kg}^{-1} \text{K}^{-1}$

| Rate (vol%)     | Lamellar dimensions |            | $\chi_c$ |           |               | Thermal properties     |            |  |
|-----------------|---------------------|------------|----------|-----------|---------------|------------------------|------------|--|
|                 | $L_c$ (nm)          | $\rho$ (%) | DSC (%)  | XRD (%)   | $\lambda$ (*) | D (*)                  | C (*)      |  |
|                 | $\pm 0.01$          | $\pm 3$    | $\pm 1$  | $\pm 0.5$ | $\pm 0.005$   | $\pm 1 \times 10^{-8}$ | $\pm 0.05$ |  |
| PEEK            |                     |            |          |           |               |                        |            |  |
|                 | 4.21                | 25         | 34       | 37.1      | 0.290         | 0.23                   | 9.81       |  |
| PEEK–BN–N       |                     |            |          |           |               |                        |            |  |
| 2.5             | 4.38                | 29         | 35       | 43.0      | 0.331         | 0.27                   | 9.41       |  |
| 5.0             | 4.40                | 29         | 36       | 46.1      | 0.371         | 0.33                   | 8.47       |  |
| 7.5             | 4.49                | 32         | 34       | 39.7      | 0.420         | 0.37                   | 8.26       |  |
| 10.0            | 4.43                | 37         | 29       | 39.8      | 0.440         | 0.57                   | 5.51       |  |
| PEEK–BN–M       |                     |            |          |           |               |                        |            |  |
| 2.5             | 4.37                | 32         | 34       | 42.5      | 0.354         | 0.27                   | 8.26       |  |
| 5.0             | 4.32                | 31         | 34       | 50.0      | 0.378         | 0.48                   | 5.91       |  |
| 7.5             | 4.37                | 31         | 35       | 39.9      | 0.431         | 0.51                   | 6.15       |  |
| 10.0            | 4.37                | 36         | 34       | 38.8      | 0.497         | 0.53                   | 6.74       |  |
| PEEK–graphite–N |                     |            |          |           |               |                        |            |  |
| 2.5             | 4.37                | 23         | 32       | 32.0      | 0.370         | 0.42                   | 6.63       |  |
| 5.0             | 4.35                | 23         | 31       | 30.6      | 0.444         | 0.40                   | 8.46       |  |
| 7.5             | 4.33                | 28         | 28       | 31.8      | 0.570         | 0.64                   | 6.52       |  |
| 10.0            | 4.33                | 29         | 29       | 29.2      | 0.690         | 0.67                   | 7.42       |  |
| PEEK–graphite–M |                     |            |          |           |               |                        |            |  |
| 2.5             | 4.43                | 26         | 33       | 32.3      | 0.390         | 0.35                   | 8.64       |  |
| 5.0             | 4.34                | 25         | 33       | 34.0      | 0.500         | 0.49                   | 7.58       |  |
| 7.5             | 4.52                | 29         | 35       | 30.7      |               |                        |            |  |
| 10.0            | 4.36                | 29         | 30       | 32.8      | 0.823         | 0.82                   | 6.65       |  |

For particulate-filled composites, the values of  $L_{\text{hkl}}$  are higher than those of PEEK. If they are all similar, it means that the influence of the addition of fillers is identical regardless of the size, type, or rate of reinforcement. Higher values of  $L_{\text{hkl}}$  indicate larger crystallite sizes. This result corroborates our interpretation of the increase in  $T_m$ .

The law of Gibbs–Thomson (Equation 2) links the lamellar thickness of crystallites  $L_c$ ,  $T_m$ , melting temperature of a 100% crystallized polymer  $T_m^{100\%}$  (for PEEK,  $T_m^{100\%} = 395^\circ\text{C}^{51}$ ), melting enthalpy of a 100% crystallized polymer  $\Delta H_m^{100\%}$ , density of crystalline phase of polymer  $\rho_c$  (for PEEK,  $\rho_c = 1.400 \text{ g cm}^{-3}$ <sup>51</sup>), and free surface energy  $\sigma_e$  (for PEEK,<sup>55</sup>  $\sigma_e = 4.9 \times 10^{-2} \text{ J m}^{-2}$ ).

$$L_c = \frac{2 \times \sigma_e \times T_m^{100\%}}{\rho_c \times \Delta H_m^{100\%} \times (T_m^{100\%} - T_m)}. \quad (2)$$

Tables 5 and 6 list the lamellae thicknesses for PEEK and PEEK composites, respectively.  $L_c$  increases with the addition of the fillers in the matrix. Adding microfillers to PEEK increases  $L_c$ , whereas there is no change with the addition of nanofillers. Again, the behavior is considerably different from that of BN. Indeed,  $L_c$  is increased with BN nanosheets; however, the increase is weaker for BN microfillers. Therefore, the lamellar thickness is higher for all composites compared to that of pure PEEK. The microfillers induce a larger crystallite size than the nanofillers, except for boron nitride.

### 3.4 | Degree of crystallinity

The degree of crystallinity was determined using several techniques: density measurement, differential scanning calorimetry, and X-ray diffraction (Tables 5 and 6). An approach to verify the strength and weakness of each technique in the analysis of the microstructure of PEEK was established in a previous study.<sup>42</sup> Tables 5 and 6 compare the degree of crystallinity for all samples with the three techniques.

The density of the matrix  $\rho_m$  is calculated using the mixing law (Equation 3) with the  $\rho$  density of the composite,  $x_r$  rate of filler, and  $\rho_r$  density of the filler.

$$\rho_m = \frac{\rho - (\rho_r \times x_r)}{1 - x_r}. \quad (3)$$

The degree of crystallinity  $\chi_c$  of the polymer from the density measurement was calculated (Equation 4) using the amorphous density ( $\rho_a = 1263 \text{ g cm}^{-3}$ ) and the crystalline density ( $\rho_c = 1400 \text{ g cm}^{-3}$ ) calculated by Blundell.<sup>51</sup>

$$\chi_c = \frac{\rho_m - \rho_a}{\rho_c - \rho_a}. \quad (4)$$

The  $\chi_c$  calculated from density measurements varies from  $19\% \pm 3\%$  to  $37\% \pm 3\%$  depending on the nature of the fillers added to the PEEK. Adding lamellar fillers in the matrix increases  $\chi_c$ . In contrast, adding particulate reinforcement decreases  $\chi_c$ .

Further,  $\chi_c$  was calculated using DSC thermograms with Formula 5. The quantities used are the experimental melting enthalpy  $\Delta H_m$  and theoretical melting enthalpy of a 100% crystalline material, for PEEK ( $\Delta H_m^{100\%} = 130 \text{ J g}^{-1}$ <sup>51</sup>).

$$\chi_c = \frac{\Delta H_m}{\Delta H_m^{100\%} \cdot x_M} \times 100. \quad (5)$$

As the conclusions are not obvious from Tables 5 and 6, the results obtained by DSC are plotted in Figure 7. Even if the rate variation is small compared to the uncertainty, it is clear that, there is no change for boron nitride in the PEEK  $\chi_c$  regardless of the size and amount of fillers. For composites with graphite,  $\chi_c$  decreased with the filler content, except at 7.5 vol%, for which  $\chi_c$  is identical to that of the PEEK matrix; this trend is more marked for nanocharges than for microcharges. For particulate fillers,  $\chi_c$  continuously decreased when filler loading increased. The effect of the size depends on the filler type: for SiC,  $\chi_c$  is always lower for microfillers than for nanofillers, and the opposite is observed for graphite. The lowest  $\chi_c$  was observed for the composite containing 7.5% SiC. The particulate fillers imply a greater drop in  $\chi_c$  compared to lamellar-type fillers. These results are consistent with previous conclusions from density measurements. From the literature, Kuo<sup>20</sup> observed a decrease in  $\chi_c$  from 5.5 wt% (i.e., 1.9 vol%) of alumina, whereas Kadiyala<sup>29</sup> observed a decrease in  $\chi_c$  of silicon carbide from 10 wt% (i.e., 4.3 vol%). No significant influence of the size on  $\chi_c$  has been mentioned in the literature. The results obtained by several authors are listed in Table 4. At low filler loadings,  $\chi_c$  increases, whereas for higher rates,  $\chi_c$  decreases. Compared with the results from the literature displayed in Table 4,  $\chi_c$  increases at a low filler loading, and it then decreases at higher rates. According to Chen,<sup>31</sup> this observation is attributed to faster crystallization with a small filler amount, compared to a higher amount. In our study, the lowest filler loading is 2.5%, which is probably not low enough to exhibit the same trend. The particulate fillers imply a greater decrease in  $\chi_c$  compared to lamellar fillers. This can be explained by the reinforcement caused by the particulate fillers on the macromolecules. One can expect that polymer mobility is reduced in the interphase close to the particulate fillers

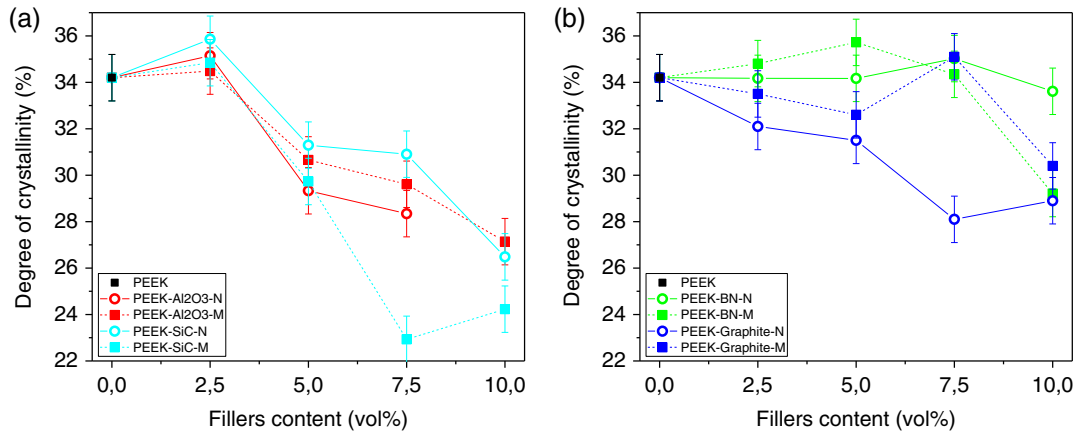


**FIGURE 7** Degree of crystallinity of composites by using differential scanning calorimetry (DSC) for polyetheretherketone reinforced with (a) particulate fillers and (b) lamellar fillers. Absolute uncertainty for degree of crystallinity determined by DSC is  $\pm 1\%$  [Color figure can be viewed at [wileyonlinelibrary.com](http://wileyonlinelibrary.com)]

because of the strong chemical interactions. On the contrary, the interphase created at the surface of the lamellar fillers is softer, which implies greater mobility, owing to the absence of chemical interactions. Boron nitride is chemically inert, and a few weak bonds are only possible at the edges of the BN sheets.

The  $\chi_c$  of PEEK was calculated using XRD to complete the analyses. The diffractogram of PEEK is typical of semi-crystalline thermoplastics, with an amorphous halo deconvoluted into five Gaussian curves. The crystalline part was deconvoluted into nine Gaussian curves. The crystalline peaks correspond to diffraction planes. The  $\chi_c$  was measured using Equation 6 by calculating the total area of the amorphous curves  $A_a$  and the total area of the crystalline curves  $A_c$ . The response coefficients of the amorphous and crystalline phases are considered equal in the calculation of  $\chi_c$  (Equation 6).

$$\chi_c = \frac{A_c}{A_c + A_a} \times 100. \quad (6)$$

However, we observed a different trend according to the filler type. No influence of size was observed on  $\chi_c$ . For composites reinforced with alumina and graphite, the addition of reinforcements reduced  $\chi_c$ . This is consistent with our previous results, wherein we assume that the molecules are more constrained and have less mobility at the interphase.

On the contrary, for composites reinforced with SiC and boron nitride, the fillers increased  $\chi_c$  up to 5 vol%, and then,  $\chi_c$  decreased in both cases at higher rates.

As the lamellae are larger than PEEK for all compositions, a decrease in  $\chi_c$  is attributed to the lower number of crystallites. One can expect that the fillers act as nucleating points to facilitate the crystallization of PEEK.

Moreover, the higher the filler amount, the higher the polymer-particle contact surface, which increases the nucleating points. As the chain mobility increases, the organization of macromolecules into the lamellae becomes easier. Thus,  $\chi_c$  is a balance between a higher number of nucleating points and reduced polymer mobility. We conclude that, when  $\chi_c$  decreases, such as for alumina and graphite, the loss of polymer mobility in the interphase is dominant compared to the contact surface caused by the fillers. Further, this is important to note that the volume of the composite analyzed is different with density, DSC, and XRD, and it can explain the difference in  $\chi_c$  according to the technique.

### 3.5 | Mechanical response

DMA is a thermomechanical technique with the unique ability to obtain insight into macromolecular chain dynamics. The composites are deformed under sinusoidal stress within the linear viscoelastic region under a heating ramp at  $3 \text{ K min}^{-1}$ . The storage modulus  $E'$  corresponds to the elastic contribution of the material's response, whereas the loss modulus  $E''$  is its viscous counterpart. The viscoelastic behavior is often expressed by the damping factor, and it is defined by  $\tan \delta = E''/E'$ .

The curves of  $E'$  for our composites are typical of filled semi-crystalline polymers, as presented in Figure 8. The storage modulus displays a plateau around 1–2 GPa in the glassy region where the segmental mobility is restricted, followed by a large  $\alpha$  relaxation, which is indicative of the glass transition of PEEK, where there is a substantial decrease in the storage modulus. Then, the rubbery plateau showing a drastic decay to 0.3 GPa is measured. The curve of the loss factor ( $\tan \delta$ ) displays a

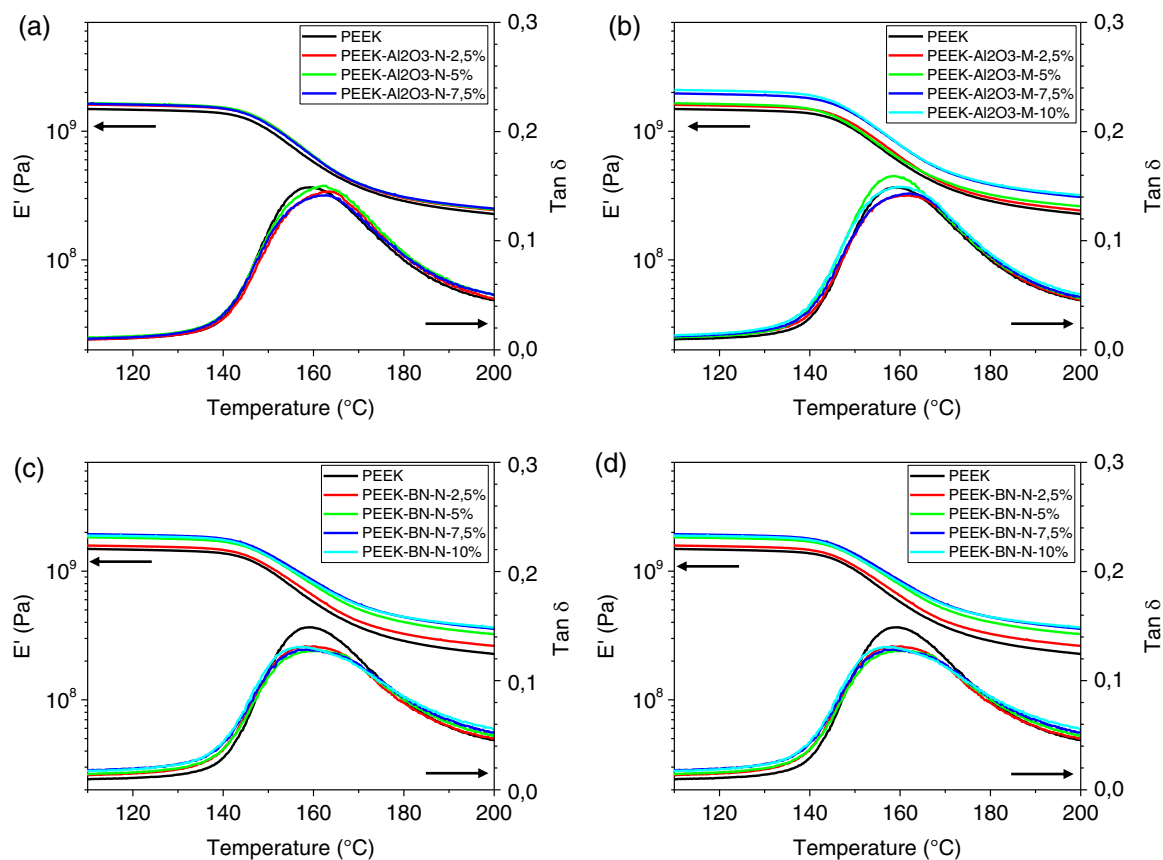


FIGURE 8 Storage modulus  $E'$  and  $\tan \delta$  of PEEK reinforced with alumina (a,b) and boron nitride (c,d) of size nanometric (a,c) and micrometric (b,d) [Color figure can be viewed at [wileyonlinelibrary.com](http://wileyonlinelibrary.com)]

broad peak, which corresponds to the  $\alpha$  relaxation. The limited movement of the side groups, which corresponds to the  $\beta$  and  $\gamma$  subrelaxations, are not visible in the temperature range that is being studied. The  $\beta$  transition occurs at  $-95^\circ\text{C}$ , and it reflects the rotation of aromatic rings and the movement of polar carbonyl bridges, which is more pronounced under humidity. In addition, a  $\gamma$  transition has been reported at a temperature of  $-155^\circ\text{C}$ , which results from localized noncooperative movements.<sup>56</sup>

Figure 8 displays the curves obtained for the nanosized (a, c) and (b, d) microsized alumina and boron nitride, respectively; however, all samples are characterized (see Supporting information). As expected, adding fillers in the PEEK matrix increases its stiffness, as attested by the increase in the storage modulus for all samples. This rising is more pronounced for microcomposites, for both alumina and boron nitride. Indeed, the  $E'$  curves of the alumina nanofilled PEEK are superimposed on one of those of the pure PEEK. In contrast, for all other formulations, the  $E'$  curves are shifted upward to higher moduli and to the right to higher temperatures. The nanoalumina does not change the chains mobility. In the case of nano boron nitride, the storage moduli are increased compared to pure PEEK; however,

the highest rising is measured for the boron nitride microfillers. This shows that the mobility of the polymeric chains is more affected in the presence of micro boron nitride.

The increase in  $E'$  stems from different factors that cannot be separated: crystallinity, particle–particle interaction, and the polymer–particle interaction.

**Crystallinity:** The storage modulus increases with crystallinity because the macromolecules are closely packed in the lamellae, which results in an increase in the compactness within the crystalline phase. As attested by Martineau,<sup>57</sup> the structural order in the crystallized PEEK material hinders the relaxation of its macromolecular chains. If we examine the crystallinity of alumina- and boron nitride-filled composites in Figure 7, the highest crystallinity is measured for the boron nitride-filled PEEK. This is consistent with the  $E'$  moduli, as the highest value of 2.84 GPa is obtained for boron nitride in the glassy state, whereas a lower  $E'$  of 2.27 GPa is measured for the alumina composites.

**Particle–particle interaction:** as expected, the storage modulus increased with the filler content. The reinforcing effect is more pronounced in the glassy state, as reported by other authors.<sup>5,46,48</sup> As verified by the SEM images, the fillers were well distributed across the sample

volume. When the filler content is increased, particles come closer to each other. From a threshold, they are very close to each other and form a percolating network. When examining the rheological behavior of such filler networks, the organization of the fillers contributes to the elastic response; its elasticity is considerably higher than the viscous contribution. The reinforcement is clearly correlated with the formation of a connected network built from finite-size primary aggregates.<sup>58</sup> We can assume that the elastic response of such a network is correlated with the elasticity of the fillers themselves. If so, the  $E'$  values of the composites would increase with an increase in their Young's modulus. The Young's modulus of alumina is 400 GPa<sup>59</sup> and that of a single boron nitride layer is 1 TPa.<sup>60</sup> Thus, the highest  $E'$  values agreed with the stiffness of the fillers.

Particle-polymer interaction: an interphase is formed near the particle surface by adding fillers in the matrix. In this interphase, macromolecules are organized differently from those in the bulk because of the interaction between the polymeric chains and filler surface. Indeed, surfaces can be attractive and molecules can be adsorbed onto the surface; the macromolecules can crystallize differently from those in the bulk. Thus, the "nano" effect is observed in filled polymers, wherein the contact surface is considerably higher for the same volume fraction.<sup>61</sup> The particle-polymer interactions near fillers result in a gain or loss of mobility for the macromolecules. The sample containing 2.5 vol% of micro boron nitride yields a curve lower than that of the matrix within the temperature range. A comparable trend was reported by Naffakh<sup>62</sup> for the addition of very low inorganic fullerene-like tungsten disulfide loadings (i.e., 0.1 wt%), which leads to a slight drop in  $E'$  (around 7% at 25°C). This is related to the decrease in crystallinity found for this sample. However, as explained above, the BN composite exhibited the highest crystallinity in our composites. Another explanation is the polymer-particle interactions. For a filler volume fraction lower than the percolation threshold, the contribution of the interphase is obvious. The decrease in  $E'$  for 2.5 vol% of micro boron nitride is attributed to the highest mobility of the macromolecules in the interphase. The surface of the boron nitride layers is chemically inert, which means that neither covalent bonds nor van der Waals bonds are expected with the PEEK matrix. As the BN content increases above 2.5 vol %, the particle-particle interaction becomes predominant in the matrix-particle interaction, which results in an increase in the storage modulus. On the contrary, chemical bonds between the alumina surface and PEEK matrix can appear. Goyal<sup>17</sup> explained that the modulus increase is attributed to the interface formed between the alumina surface and the matrix.

Now, let us view the shape of the  $\tan \delta$  peak in Figure 8. There is a slight change in the maximum width of the peak for nanoalumina compared to pure PEEK, while this difference is accentuated for the other samples. Indeed, the maximum of the  $\tan \delta$  peak indicates the transition from a restricted (glassy state) to a mobile amorphous state. Adding fillers affects the damping factor by shifting the peak location and broadening the peak. The shift in position is attributed to the presence of an interphase wherein the macromolecules are organized in a different way compared to the bulk. The interphase results from the creation of chemical bonds at the filler-polymer interface. Macromolecules located in this interphase are closely packed, and their mobility is reduced compared to that of the mobile amorphous phase of the bulk. The magnitude of the  $\tan \delta$  peak is often assigned to the filler-matrix interactions. For instance, Naffakh<sup>62</sup> observed that the height of the  $\tan \delta$  peak decreases with increasing inorganic fullerene-like tungsten disulfide content, which is explained by a strong nanofiller-matrix interfacial adhesion and from a synergistic effect between the fillers on restricting chain mobility. In addition, Chen<sup>48</sup> explained the peak decrease caused by a reduction in mobility near the particles. For higher accuracy, the width of the peak must be thoroughly analyzed, and the broadening of  $\tan \delta$  is attributed to the contribution of the interfacial effects at the polymer-filler interface. Unlike the restricted amorphous fraction, the polymer immobilized on the filler surface affects the relaxation dynamics.<sup>63</sup> For nanoalumina, the peak becomes more asymmetric with increasing nanoparticle loading; it is unchanged on the left side, whereas it broadens towards higher temperatures. This can be attributed to the contribution of the nanofiller-matrix adhesion, which is another indication of the larger nanoparticle-matrix interfacial area. For all other samples, the width of the  $\tan \delta$  peak becomes broader on both sides as the filler content increases. On the left, this can be attributed to higher chain mobility near the filler contact surface caused by an increase in the free volume. On the right, this broadening can be interpreted as the elastic contribution of the particle network.

### 3.6 | Thermal properties

Thermal conductivity, thermal diffusivity, and heat capacity were measured for PEEK and each of the composite materials used in this study. Thermal conductivity represents the ability of the material to transport thermal energy from near to near. The thermal diffusivity represents the capacity to distribute this thermal energy nearly rapidly and homogeneously in the material; therefore, it



depends strongly on the homogeneity of the material. Finally, the mass heat capacity is associated with the thermal energy required to raise the temperature of the material by 1 K per unit mass. Further, it reflects the degree of freedom of the elementary constituents of the material, and the higher the heat capacity, the more vibration, rotation, and deformation phenomena come into play at the molecular level. These three thermal properties are related because thermal conductivity is a product of the density with thermal diffusivity and mass heat capacity. They are all displaced in Tables 5 and 6.

Since the thermal conductivities of fillers are higher than that of PEEK, which is  $0.29 \text{ W m}^{-1} \text{ K}^{-1}$ , the composites have a higher conductivity than the virgin matrix. The mixing law does not support our results well because of the contribution of several physical phenomena. Thermal transfer does indeed stem from phonon displacement and electron transport. In addition, interfacial adhesion plays a major role because heat transfer from the matrix to the fillers is better when there is strong adhesion. For PEEK reinforced with 7.5 vol% of the nanofiller of alumina and 7.5 vol% of the microfiller of graphite, the specimens were too thin to perform measurements; therefore, they are not presented. The general trends indicate an increase in the thermal diffusivity and a decrease in the heat capacity with the addition of fillers. Further,  $\lambda$  increased with filler loading. However, the thermal diffusivity and heat capacity of PEEK loaded with 7.5 vol% of silicon carbide nanoparticles or 5 vol% of graphite nanofillers do not follow the generally observed trends. This can be attributed to the inhomogeneous distribution of fillers in the matrix (Figure 9).

Materials containing spherical fillers (silicon carbide or alumina):  $\lambda$  increases with filler content from 0.295 to

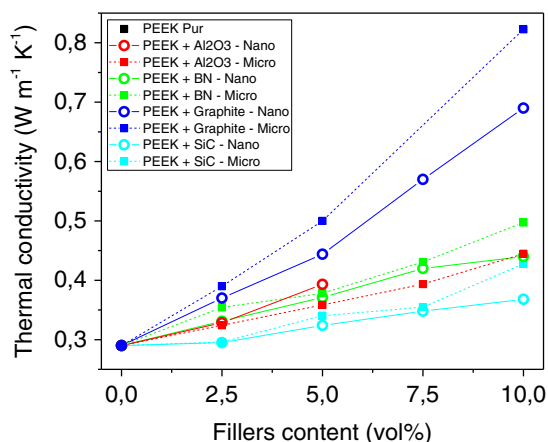


**FIGURE 9** Thermal conductivity for samples reinforced with alumina, boron nitride, graphite and silicon carbide. Lines correspond to theoretic density of samples. Absolute uncertainty for density measurement is  $0.01 \text{ W m}^{-1} \text{ K}^{-1}$ , not shown on the graph [Color figure can be viewed at [wileyonlinelibrary.com](http://wileyonlinelibrary.com)]

$0.445 \text{ W m}^{-1} \text{ K}^{-1}$ . Meanwhile, the thermal diffusivity of the composites increases significantly, from  $2.5 \text{ \AA}—10^{-7} \text{ m}^2 \text{ s}^{-1}$ . The addition of nanoscale silicon carbon led to the most noticeable increase in the thermal diffusivity. Therefore, silicon carbide nanoparticles contribute to the most efficient heat diffusion in this series of materials. Finally, the heat capacity varies slightly with the addition of SiC or the alumina filler. However, SiC nanoparticles promote a significant lowering of the heat capacity, which is consistent with a decrease in the intramolecular mobility caused by the presence of SiC nanoparticles. The 2.5 vol% content of micrometric silicon carbide also causes this drop in heat capacity; however, this effect quickly fades with the addition of the filler. The thermal properties stay moderated with the formulations with spherical particles, because the percolation threshold is not reached at these loadings. Indeed, when the spherical particles are uniformly distributed inside the matrix, a large concentration is necessary to form a percolating network. Further, these composites cannot be prepared by melt mixing because of their extremely high viscosities.

Materials containing lamellar fillers:  $\lambda$  increases more significantly, from  $0.331 \text{ W m}^{-1} \text{ K}^{-1}$  with 2.5 vol% of boron nitride and up to  $0.497 \text{ W m}^{-1} \text{ K}^{-1}$  with 10 vol% of boron nitride. We measured  $0.823 \text{ W m}^{-1} \text{ K}^{-1}$  with 10 vol% of micrometric graphite. An increase in thermal diffusivity is accompanied by an increase in the particle content and a decrease in the heat capacity by mass. The addition of lamellar particles increases the ability of the material to transport heat efficiently and homogeneously throughout the volume; however, this is at the expense of intramolecular mobility. As attested by the DMA results, the lamellar fillers are organized into percolating networks, and therefore, the paths created by additional fillers seem to cause an improvement in the thermal conductivity of these materials. The highest  $\lambda$  was obtained with graphite, whereas the results for boron nitride were below the expectation despite its in-plane conductivity at approximately  $400 \text{ W m}^{-1} \text{ K}^{-1}$ . Graphite and boron nitride have a very similar structure with an interlayer spacing of 0.34 nm and interlayer energy bonding<sup>64,65</sup> at  $0.33 \text{ J m}^{-2}$ . The only difference is that delocalized  $\pi$  electrons are present in graphite, which explains the thermal properties of graphite-based composites. The increase in the particle size contributes to an increase in  $\lambda$  regardless of the nature of the fillers. This result is consistent with Luo's study,<sup>66</sup> who studied the influences of graphene size, interfacial bonding strength, and polymer density on the interfacial thermal transport. According to his molecular dynamics simulation, he found that thermal energy transport across graphene/graphite polymer interfaces can be enhanced by

increasing the polymer density and graphene size or by forming covalent bonds between the graphite and the matrix.

## 4 | SUMMARY

For  $T_m$ , the maximum shift was  $2.6^\circ\text{C}$  with the addition of fillers. The  $T_c$  shifted to a higher temperature for nanosized boron nitride and downward for nanosized alumina. The variation in  $T_c$  was larger for nanofillers than that for microfillers. The DSC tests indicated a slight change in  $T_g$ . With the addition of alumina,  $T_g$  decreased compared to that of pure PEEK. For other fillers,  $T_g$  increased for the lowest rate of fillers and decreased for the

highest rate of fillers. The nature and rate of reinforcement influenced  $T_g$ . These results suggest that the size of the filler is a dominant factor in the evolution of thermal transitions compared to the nature and filler content.

The  $\chi_c$  increased with lamellar fillers, whereas a reduction in  $\chi_c$  was measured with particulate fillers. This stems from the interphase created by polymer-particle interactions, wherein macromolecules are more constrained than that in the bulk. Indeed, strong chemical bonds were created between alumina and PEEK, whereas no chemical interactions occurred at the boron nitride surface. Even if the addition of fillers increased the interfacial area between the matrix and fillers, the nucleating effect was hindered by the mobility of the chains. At low contents, such as 2.5 vol%,  $\chi_c$

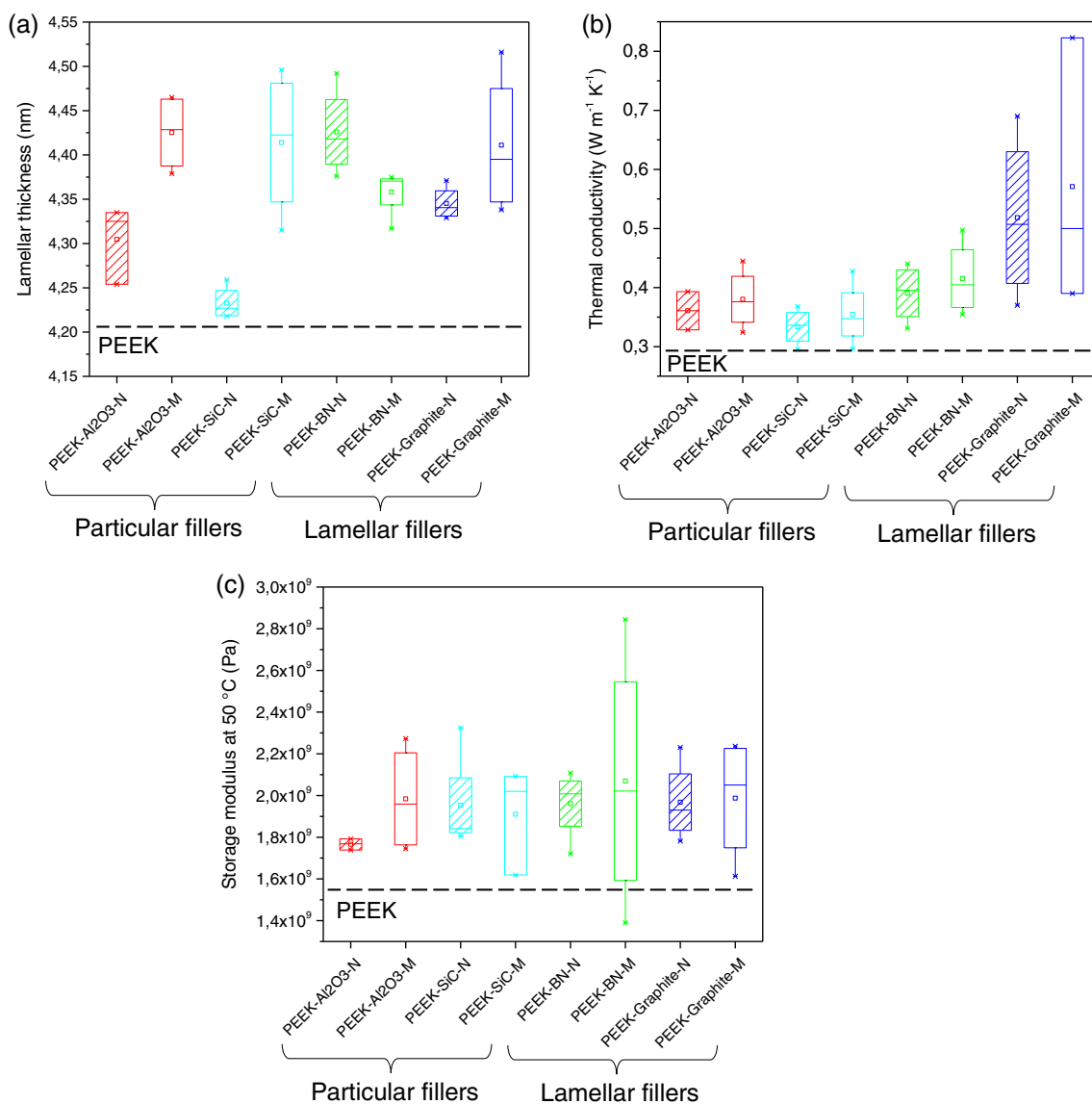


FIGURE 10 Summary of the effect of nature and size of fillers in polyetheretherketone composites [Color figure can be viewed at [wileyonlinelibrary.com](http://wileyonlinelibrary.com)]

increased. At higher contents, macromolecules are too constrained by the fillers to self organize into spherulites, and  $\chi_c$  is influenced by the nature and rate of the fillers.

Figure 10a compares the evolution of the lamellar thickness for PEEK reinforced. This representation estimates the influence of the size and the nature of the fillers; however, no direct estimation can be drawn for the influence of the rate of the fillers. The lamellar thickness is 4.21 nm for PEEK and is represented with a dashed line. For particulate fillers, the lamellar thickness of the spherulites increases more with micro size than with nano size. With lamellar fillers,  $L_c$  increases by at most 4.51 nm. No difference occurs between nano and micro sizes.

Figure 10b highlights the systematic increase of  $\lambda$  by adding reinforcements. As predicted, fillers with higher  $\lambda$  such as graphite increase the  $\lambda$  of the composite. Moreover, the rate of reinforcement increases linearly with the increase in thermal conductivity. Size seems to influence the thermal properties slightly.  $\lambda$  was higher for the micro sized fillers because of the increase in the lamellar thickness that enhanced the thermal conductivity. However, the  $\lambda$  of the filler is an important parameter for the evolution of the thermal properties of the composite. The rate and size of fillers modify thermal properties. In conclusion, if we want to increase thermal properties, we need to add a considerable amount of conductive fillers.

Figure 10c shows the increase in the storage modulus  $E'$  obtained by adding reinforcements at 50°C. With nanofillers, the dispersion of the values is less important than that with microfillers. As expected, adding fillers enhances the storage modulus  $E'$  and the loss modulus  $E''$  because of the higher Young's modulus of the fillers and higher fillers rigidity: around 400 GPa for particulate fillers<sup>59,67</sup> and superior to 1 TPa for lamellar fillers.<sup>60,68</sup> The increase in the storage modulus  $E'$  is proportional to the filler concentration. The nature of fillers is not sufficiently discriminant for estimating a change in the storage modulus.

## 5 | CONCLUSIONS

In this work, we prepared 32 PEEK micro- and nanocomposites by melt blending. To the best of our knowledge, this is the first study to compare four types of fillers: two particulate fillers (silicon carbide and alumina) and two lamellar fillers (boron nitride and graphite). All fillers have a considerably higher  $\lambda$  than that of pure PEEK. We aimed to connect the thermal properties to the morphology of the composites. This work contributes to a better understanding of PEEK composites and the prediction of their properties by studying their size, concentration, nature, and fillers. The filler content was confirmed using density measurements. The thermal

transitions and lamellar thicknesses were obtained by DSC. The morphology and polymer dynamics were assessed by DMA, and finally, the thermal properties of the composites were measured using a hot disk. The main conclusions are summarized below.

1. For the largest fillers,  $L_c$  is bigger. The nature of the fillers has no impact on the lamellar thickness.
2. The fillers are organized in a percolating network that contributes greatly to the elastic rheological response of composites, which means that the particle-particle interaction dominates. Consequently, the elastic modulus is improved with the filler content.
3. The effect of filler size on rheological properties is low because the particle-polymer interaction is hidden by the particle-particle interaction.
4. The composite containing 10 vol% of boron nitride achieved the highest storage modulus in the glassy region. This was explained by the stiffness caused by the rigid particle network in the free amorphous phase. Boron nitride layers provide more mobility to the macromolecules in the interphase, which is the area close to the filler surface.
5. As expected,  $\lambda$  was improved by increasing the filler content. The highest conductivity was achieved for the lamellar fillers. Indeed, the shape ratio (length/width) was larger for lamellar fillers, and therefore, the percolating network was formed at a lower concentration than that for particulate fillers with quasi-spherical geometry. Further, using micrometric fillers enhanced  $\lambda$  because of the higher amount of more efficient hot zones for heat transfer. These results showed that the nature of fillers has a greater influence on the rheological and thermal properties than content and size.

## ACKNOWLEDGMENTS

The Occitanie region of France and the Université Fédérale de Toulouse-France supported this research through a PhD funding (APR no ALDOC-000185-2017 001834).

## ORCID

Florentin Berthet  <https://orcid.org/0000-0003-1264-7402>

Karl Delbé  <https://orcid.org/0000-0002-8503-2671>

Olivier Marsan  <https://orcid.org/0000-0002-9338-4052>

Jean Denape  <https://orcid.org/0000-0002-0496-9447>

France Chabert  <https://orcid.org/0000-0001-6309-4372>

## REFERENCES

- [1] D. A. Jesson, J. F. Watts, *Polym. Rev.* **2012**, 52, 321. <https://doi.org/10.1080/15583724.2012.710288>
- [2] Y. Liu, S. Kumar, *ACS Appl. Mater. Interfaces* **2014**, 6, 6069. <https://doi.org/10.1021/am405136s>
- [3] T. E. Attwood, P. C. Dawson, J. L. Freeman, L. R. J. Hoy, J. B. Rose, P. A. Staniland, *Polymer* **1981**, 22, 1096.
- [4] A. P. Harsha, U. S. Tewari, *Polym. Test.* **2002**, 21, 697.

- [5] A. M. Diez-Pascual, J. Guan, B. Simard, M. A. GÃ3mez-Fatou, *Compos. A: Appl. Sci. Manuf.* **2012**, *43*, 1007.
- [6] R. Schroeder, F. W. Torres, C. Binder, A. N. Klein, J. D. B. de Mello, *Wear* **2013**, *301*, 717.
- [7] V. Rodriguez, J. Sukumaran, A. K. Schlarb, P. D. Baets, *Wear* **2016**, *362–363*, 161.
- [8] J. N. Panda, J. Bijwe, R. K. Pandey, *Compos. Sci. Technol.* **2018**, *167*, 7.
- [9] L. Guo, G. Zhang, D. Wang, F. Zhao, T. Wang, Q. Wang, *Compos. A: Appl. Sci. Manuf.* **2017**, *102*, 400.
- [10] D. N. Bikiaris, G. Z. Papageorgiou, E. Pavlidou, N. Vouroutzis, P. Palatzoglou, G. P. Karayannidis, *J. Appl. Polym. Sci.* **2006**, *100*, 2684. <https://doi.org/10.1002/app.22849>
- [11] S. Javaid, M. Dey, N. Kaabouch, S. Gupta, *J. Appl. Polym. Sci.* **2021**, *138*, 49980. <https://doi.org/10.1002/app.49980>
- [12] K. V. Mahesh, S. Balanand, R. Raimond, A. P. Mohamed, S. Ananthakumar, *Mater. Des.* **2014**, *63*, 360.
- [13] J. Chen, Q. Guo, Z. Zhao, X. Shao, X. Wang, C. Duan, *J. Appl. Polym. Sci.* **2013**, *127*, 2220. <https://doi.org/10.1002/app.37923>
- [14] R. Ramani, S. Alam, *J. Appl. Polym. Sci.* **2012**, *125*, 3200. <https://doi.org/10.1002/app.36501>
- [15] Q.-J. Xue, Q.-H. Wang, *Wear* **1997**, *213*, 54.
- [16] R. K. Goyal, Y. S. Negi, A. N. Tiwari, *J. Appl. Polym. Sci.* **2006**, *100*, 4623. <https://doi.org/10.1002/app.23083>
- [17] R. Goyal, A. Tiwari, U. Mulik, Y. Negi, *Compos. Sci. Technol.* **2007**, *67*, 1802.
- [18] J. Tharajak, T. Palathai, N. Sombatsompop, *Surf. Coat. Technol.* **2015**, *273*, 20.
- [19] A. K. Kadiyala, J. Bijwe, *Compos. Sci. Technol.* **2018**, *155*, 177.
- [20] M. C. Kuo, C. M. Tsai, J. C. Huang, M. Chen, *Mater. Chem. Phys.* **2005**, *90*, 185.
- [21] S. R. Kim, D. H. Kim, D. J. Kim, M. H. Kim, J. M. Park, *Solid State Phenom.* **2007**, *124–126*, 1079.
- [22] A. Tewatia, J. Hendrix, Z. Dong, M. Taghon, S. Tse, G. Chiu, W. E. Mayo, B. Kear, T. Nosker, J. Lynch, *Mater. Sci. Eng. B* **2017**, *216*, 41.
- [23] Y. Shang, Y. Zhao, Y. Liu, Y. Zhu, Z. Jiang, H. Zhang, *High Perform. Polym.* **2018**, *30*, 153. <https://doi.org/10.1177/0954008316685410>
- [24] G. Liu, L. Zhang, G. Li, F. Zhao, Q. Che, C. Wang, G. Zhang, *Acta Biomater.* **2019**, *87*, 285.
- [25] M. Zalaznik, M. Kalin, S. Novak, *Tribol. Int.* **2016**, *94*, 92.
- [26] W. Zhou, S. Qi, Q. An, H. Zhao, N. Liu, *Mater. Res. Bull.* **2007a**, *42*, 1863.
- [27] W. Zhou, S. Qi, H. Li, S. Shao, *Thermochim. Acta* **2007b**, *452*, 36.
- [28] J. A. Puertolas, M. Castro, J. A. Morris, R. Rios, A. Anson-Casaos, *Carbon* **2019**, *141*, 107.
- [29] A. K. Kadiyala, J. Bijwe, P. Kalappa, *Surface Coat. Technol.* **2018**, *334*, 124.
- [30] R. K. Goyal, A. N. Tiwari, Y. S. Negi, *Mater. Sci. Eng. A* **2008**, *486*, 602.
- [31] B. Chen, S. Berretta, K. Evans, K. Smith, O. Ghita, *Appl. Surf. Sci.* **2018**, *428*, 1018.
- [32] S. Abbasi, P. Carreau, A. Derdouri, M. Moan, *Rheol. Acta* **2009**, *48*, 943. <https://doi.org/10.1007/s00397-009-0375-7>
- [33] Victrex Data Sheet Victrex PEEK 450G (Revision November 2019). Available from <https://www.victrex.com/en/products/polymers/peek-polymers>
- [34] M. Bodaghi, H. Zolfonoon, M. Tahriri, M. Karimi, *Solid State Sci.* **2009**, *11*, 496.
- [35] X. Li, X. Chen, H. Song, *Mater. Sci. Eng. B* **2011**, *176*, 87.
- [36] Z. Cui, A. Oyer, A. Glover, H. Schniepp, D. Adamson, *Small* **2014**, *10*, 2352. <https://doi.org/10.1002/sml.201303236>
- [37] A. Naseri, A. D. Sediako, F. Liu, M. Barati, R. D. Baker, M. J. Thomson, *Carbon* **2020**, *156*, 299.
- [38] R. Zouari, T. Domenech, B. Vergnes, E. Peuvrel-Disdier, *J. Rheol.* **2012**, *56*, 725. <https://doi.org/10.1122/1.4708602>
- [39] T. Domenech, R. Zouari, B. Vergnes, E. Peuvrel-Disdier, *Macromolecules* **2014**, *47*, 3417. <https://doi.org/10.1021/ma5001354>
- [40] G. Normand, E. Peuvrel-Disdier, B. Vergnes, *Int. Polym. Process.* **2016**, *31*, 508.
- [41] Y. Xian, Z. Kang, X. Liang, *J. Appl. Polym. Sci.* **2021**, *138*, 50496. <https://doi.org/10.1002/app.50496>
- [42] M. Doumeng, L. Makhlof, F. Berthet, O. Marsan, K. Delbe, J. Denape, F. Chabert, *Polym. Test.* **2021**, *93*, 106878.
- [43] R. Goyal, Y. Negi, A. Tiwari, *Eur. Polym. J.* **2005**, *41*, 2034.
- [44] J. Tharajak, T. Palathai, N. Sombatsompop, *Surf. Coat. Technol.* **2017**, *321*, 477.
- [45] M. He, X. Chen, Z. Guo, X. Qiu, Y. Yang, C. Su, N. Jiang, Y. Li, D. Sun, L. Zhang, *Compos. Sci. Technol.* **2019**, *174*, 194.
- [46] V. Balaji, A. N. Tiwari, R. K. Goyal, *J. Appl. Polym. Sci.* **2011**, *119*, 311. <https://doi.org/10.1002/app.32750>
- [47] M. Bragaglia, V. Cherubini, F. Nanni, *Compos. Sci. Technol.* **2020**, *199*, 108365.
- [48] B. Chen, B. Yazdani, L. Benedetti, H. Chang, Y. Zhu, O. Ghita, *Compos. Sci. Technol.* **2019**, *170*, 116.
- [49] J. N. Panda, J. Bijwe, R. K. Pandey, *Compos. B Eng.* **2019**, *174*, 106951.
- [50] P. C. Dawson, D. J. Blundell, *Polymer* **1980**, *21*, 577.
- [51] D. J. Blundell, B. N. Osborn, *Polymer* **1983**, *24*, 953.
- [52] A. Reyna-Valencia, S. Kaliaguine, M. Bousmina, *J. Appl. Polym. Sci.* **2006**, *99*, 756. <https://doi.org/10.1002/app.22551>
- [53] B. S. Hsiao, B. B. Sauer, A. Biswas, *J. Polym. Sci. B Polym. Phys.* **1994**, *32*, 737. <https://doi.org/10.1002/polb.1994.090320415>
- [54] J. N. Hay, J. I. Langford, J. R. Lloyd, *Polymer* **1989**, *30*, 489.
- [55] E. Courvoisier, Y. Bicaba, X. Colin, *Polym. Degrad. Stab.* **2018**, *151*, 65.
- [56] L. David, S. Etienne, *Macromolecules* **1992**, *25*, 4302. <https://doi.org/10.1021/ma00043a010>
- [57] L. Martineau, F. Chabert, G. Bernhart, T. Djilali. in ECCM17 - 17th European Conference on Composites Materials. (2016). <https://hal.archives-ouvertes.fr/hal-01515536/document>.
- [58] N. Jouault, P. Vallat, F. Dalmas, S. Said, J. Jestin, F. Boue, *Macromolecules* **2009**, *42*, 2031. <https://doi.org/10.1021/ma801908u>
- [59] K. Suganuma, T. Fujita, N. Suzuki, K. Niihara, *J. Mater. Sci. Lett.* **1990**, *9*, 633. <https://doi.org/10.1007/BF00721787>
- [60] J. Joy, E. George, P. Haritha, S. Thomas, S. Anas, *J. Polym. Sci.* **2020**, *58*, 3115. <https://doi.org/10.1002/pol.20200507>
- [61] A. J. Crosby, Y. Lee, *Polym. Rev.* **2007**, *47*, 217. <https://doi.org/10.1080/15583720701271278>
- [62] M. Naffakh, A. Diez-Pascual, *Inorganics* **2014**, *2*, 291.
- [63] B. H. Soudmand, K. Shelesh-Nezhad, Y. Salimi, *J. Appl. Polym. Sci.* **2020**, *137*, 49260. <https://doi.org/10.1002/app.49260>
- [64] W. Wang, S. Dai, X. Li, J. Yang, D. J. Srolowitz, Q. Zheng, *Nat. Commun.* **2015**, *6*, 7853.

- [65] O. Hod, *J. Chem. Theory Comput.* **2012**, 8, 1360. <https://doi.org/10.1021/ct200880m>
- [66] T. Luo, J. R. Lloyd, *Adv. Funct. Mater.* **2012**, 22, 2495. <https://doi.org/10.1002/adfm.201103048>
- [67] N. G. Wright, *Kirk Othmer Encyclopedia of Chemical Technology*. John Wiley & Sons, Inc., Hoboken. **2000**. <https://doi.org/10.1002/0471238961>
- [68] A. S. Fedorov, Z. I. Popov, D. A. Fedorov, N. S. Eliseeva, M. V. Serjantova, A. A. Kuzubov, *Phys. Status Solidi B* **2012**, 249, 2549. <https://doi.org/10.1002/pssb.201200105>

## SUPPORTING INFORMATION

Additional supporting information may be found in the online version of the article at the publisher's website.